Journal of Ovonic Research Vol. 19, No. 4, July - August 2023, p. 439 - 451

Synthesis and characterization of some Cr-Zr and Cr-Zr-O nanostructures

V. Ciupina[a,b,d], M. Albu[a], A. Caraiane[a], C. Porosnicu[c], C. Staicu[b,c], P. Dinca[c], V. Nicolescu[e], R. Manu[f,*]

[a]*Ovidius University of Constanta, 124 Mamaia Ave., 900527, Constanta, Romania*
[b]*Faculty of Physics, The University of Bucharest, 405 Atomistilor St., PO Box MG-11, RO – 077125, Magurele, Ilfov, Romania*
[c]*National Institute for Laser, Plasma and Radiation Physics, 409C Atomistilor St., PO Box MG-36, 077125, Magurele, Ilfov, Romania*
[d]*Academy of Romanian Scientists, Splaiul Independentei St, No. 54, 050094, Bucharest, Romania*
[e]*CERONAV, 69A Pescarilor St., 900581, Constanta, Romania*
[f]*Naval Academy ,,Mircea cel Batran'', Fulgerului No.1, 900218, Constanta, Romania*

The co-depositions of Cr-Zr and those of Cr-Zr-O coatings of 500 nm thick were made using magnetron sputtering in continuous mode, in a circular enclosure with a volume of 0.05 m^3 evacuated prior to the deposition process under 10^{-6} mbar vacuum conditions. Silicon and Carbon substrates measuring 12x15mm were used for deposition. The topology of all of the CrZr and $CrZrO_2$ coatings deposited on silicon and carbon substrates have been investigated by Scanning Electron Microscopy (SEM) at three magnifications: 1000x, 5000x and 10.000x. For all of the coatings deposited on Silicon substrates, at all three magnifications, was observed very smooth surfaces with only small topological elements. In some samples, few droplets of around 100nm can be observed. The appearance of particulates is caused by the arching events that occur at target surface during the deposition proces and are more pronounced during reactive sputtering. The coatings deposited on the Carbon substrate show more morphological features as these substrates have a lower grade surface polish finish as to sliced Silicon wafers; the deposited film tends to follow the substrate topology and cracks can be seen on the surface. Were investigated the mechanical properties of the samples of Cr+Zr, respectively $Cr+Zr+O_2$ using The Bruker Hysitron TI 980 TriboIndenter which allows to extrapolate mechanical properties such Young's Modulus (YM) and Hardness (H). The experimental results obtained through nanoindentation studies, show: In the absence of oxygen during deposition (Zr-Cr structures), the Young's Modulus and Hardness are influenced by the concentration ratio of the two components Cr and Zr, i.e., there is the practical possibility of adjusting the two parameters YM and H by correspondingly changing the concentrations of the components of the structure . In the case of the $Cr+Zr+O_2$ structures, for sample where the concentration of Chromium is maximum and the concentration of Zirconium is minimum, the presence of Oxygen causes a decrease for YM and respectively a decrease for H (in this case Cr-O bonds are predominant). In the case of sample in which the concentration of Zirconium is maximum and the concentration of Chromium is minimum, in the presence of Oxygen (now the bonds Zr-O being predominant), an increase for YM and an increase for H are observed. The crystalline structure was investigated using X-Ray Diffraction (XRD) method, using a set-up composed of a diffractometer equipped with a Cu-Kα X-ray sourse, with a specific wavelength of 0.154nm, in a Bragg-Bretano type geometry. In the case of the Cr-Zr sample, diffractograms show that only the peaks corresponding to the Si substrate are visible, highlighting the amorphous character of the structure. Also, the measurements reveal the amorfous character of the Cr-Zr-O sample. In order to highlight the effect of the element Cr together with Zr and O, the diffractogram of the ZrO_2 sample and diffractogram of Cr-Zr-O sample are examinated for comparison. Considering the application of these materials in dentistry, the 2 wide amorphous strips in the case of ZrO_2 sample and amorfous character found in the case of Cr-Zr-O sample, could correspond to the adhesive used to attach the veneer to the tooth of such structures. From this perspective, it can be stated that the presence of the Cr element in the Cr-Zr-O structure widens the possibility of its use as an adhesive to attach the veneer to the tooth.

(Received June 7, 2023; Accepted August 1, 2023)

Keywords: CrZr, $CrZrO_2$, Magnetron sputtering, SEM, Nanoindentation, XRD

* Corresponding author: radu.manu@anmb.ro
https://doi.org/10.15251/JOR.2023.194.439

1. Introduction

The development of oxide-based thin film materials for different applications is currently attracting large interest. Besides the theoretical modeling of structural design and properties of such materials the systematic evaluation of plasma-based deposition methods for their synthesis will contribute to create an important data base for advanced materials development. In this context, the Cr–Zr–O system has been intensively studied. Thus, was observed that monoclinic ZrO_2 is able to dissolve Cr_2O_3 without structural changes until the volume of the unit cell fell to a certain value. Among the synthesis methods, RF reactive magnetron sputtering becomes one of the most popular technique for the preparation of Cr-Zr-O coatings. Unfortunately, studies on Cr-Zr-O coatings are limited. Thus, Spitz et al. prepared Cr-Zr-O films with different Cr and Zr contents at 500 °C by RF magnetron sputtering, and studied the effects of composition and annealing temperature on the microstructure and properties of the films [1],[2]. The structural evolution and properties of Cr-Zr-O coatings under different annealing temperatures are investigated also by L. Landälv et al. [3].In this case, reactive RF-magnetron sputtering is used to grow Cr0.28Zr0.10O0.61 coatings at 500 °C. Coatings with superior hardness, high temperature thermal stability, and oxidation resistance, required to protect cutting tools in machining applications, were synthesed by M. Mohammadtaheri et al. [4],[5]. The synthesis of such coatings was investigated in a ternary Cr–Zr–O system by reactive radio-frequency magnetron sputtering technique. A new coating system of Zr-Cr-O in which tetragonal ZrO_2 [6],[7],[8],[9] acts as toughening agent and Cr_2O_3 can act as stabilizer and hard matrix was proposed by Kai Huang et al [10]. The coatings were obtained by cathodic arc deposition of Zr and Cr in gas mixture of oxygen and argon. The hardness of the coatings was affected by composition, substrate bias and crystallinity. Our paper presents some Cr-Zr and Cr-Zr-O nanostructures obtined by magnetron sputtering in continuous mode technology.

2. Experimental set-up

The co-depositions of Cr+Zr and those of Cr+Zr+O_2 coatings of 500 nm thick were made using magnetron sputtering in continuous mode, in a circular enclosure with a volume of 0.05 m^3 evacuated prior to the deposition process under 10^{-6} mbar vacuum conditions by using a turbomolecular pump. The experimental scheme of the deposition chamber is represented in Fig.1. Substrates of Si and C with (12x15mm) sizes were used for deposition. They were cleaned by ultrasonication in a mixture of isopropyl alcohol and acetone to remove impurities. Afterwards the substrates were washed abundantly with distilled water and then allowed to dry in atmospheric air. Finally the substrates were mounted in the chamber on a fixed circular support positioned at a distance of approximately 10 cm from the spray source.

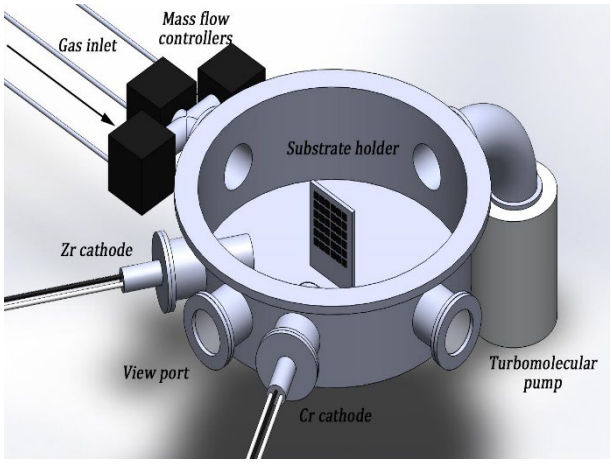

Fig. 1. Deposition chamber.

The magnetron systems used were composed of a water-cooled cathode equipped with circular Cr/Zr targets (2 mm thick and 50 mm diameter) of high purity (99.95%). Throughout the experiments, the pressure was kept constant at a value of 10^{-2}mbar. The two gas flows, for Ar and for O_2, were 20 sccm. The Tab.1 shows the deposition parameters (drop potential U, curent intensity I, and ratio of the curent R) for the two materials of interest for deposition without O_2 inclusions.

Table 1. Working parameters for Cr+Zr deposition.

Cr	Zr
U= 0.29 kV	U= 0.23 kV
I= 0.05 A	I= 0.12 A
R = 0.40 A/s	R = 0.8 A/s

In Table 2 are presented the deposition parameters for the two materials of interest for deposition with O_2 inclusions.

Table 2. Working parameters for Cr+Zr +O_2 deposition.

Cr	Zr
U= 0.36 kV	U= 245 V
I= 0.25 A	I= 0.60 mA
R = 0.1 A/s	R = 0.2 A/s

3. Results and discussions

In order to have a picture of the influence of the material on the characteristics of the two types of samples (Cr+Zr with or without O_2 inclusions), 5 Si and 1 C substrates placed in line were used (Fig.2).

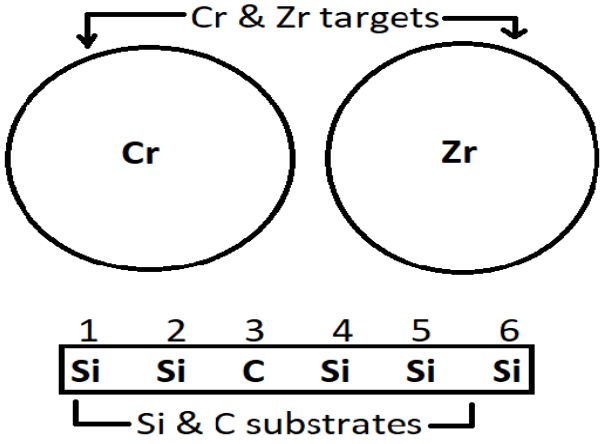

Fig. 2. Scheme of deposition.

The samples are marked as follows: Si_1, Si_2 and C_3 positioned towards the Cr target, so we expect the Cr concentration to be higher. While Si_4, Si_5 and Si_6 are towards the Zr target, which causes the Zr concentration to increase. Moreover, since it is about two depositions, the first without oxygen and the second with oxygen, samples will be marked as follows: Si_1_A,

Si_2_A, C_3_A, Si_4_A, Si_5_A and Si_6_A (A representing deposition without oxygen); Si_1_B, Si_2_B, C_3_B, Si_4_B, Si_5_B and Si_6_B (B representing deposition with oxygen).

3.1. SEM studies

The topology of all of the CrZr and $CrZrO_2$ coatings deposited on silicon and carbon substrates have been investigated by Scanning Electron Microscopy (SEM) using a FEI Inspect S scanning electron microscope (Hillsboro, Oregon, OR, USA) in low-vacuum mode at three magnifications: 1000x, 5000x and 10.000x. For all of the coatings deposited on Si substrates, at all three magnifications, we observe very smooth surfaces with only small topological elements as we can see in Fig.3 for samples Si_4_A (at 10kx magnification), Si_5_A (at 5kx magnification), and Si_6_B (at 10kx magnification).

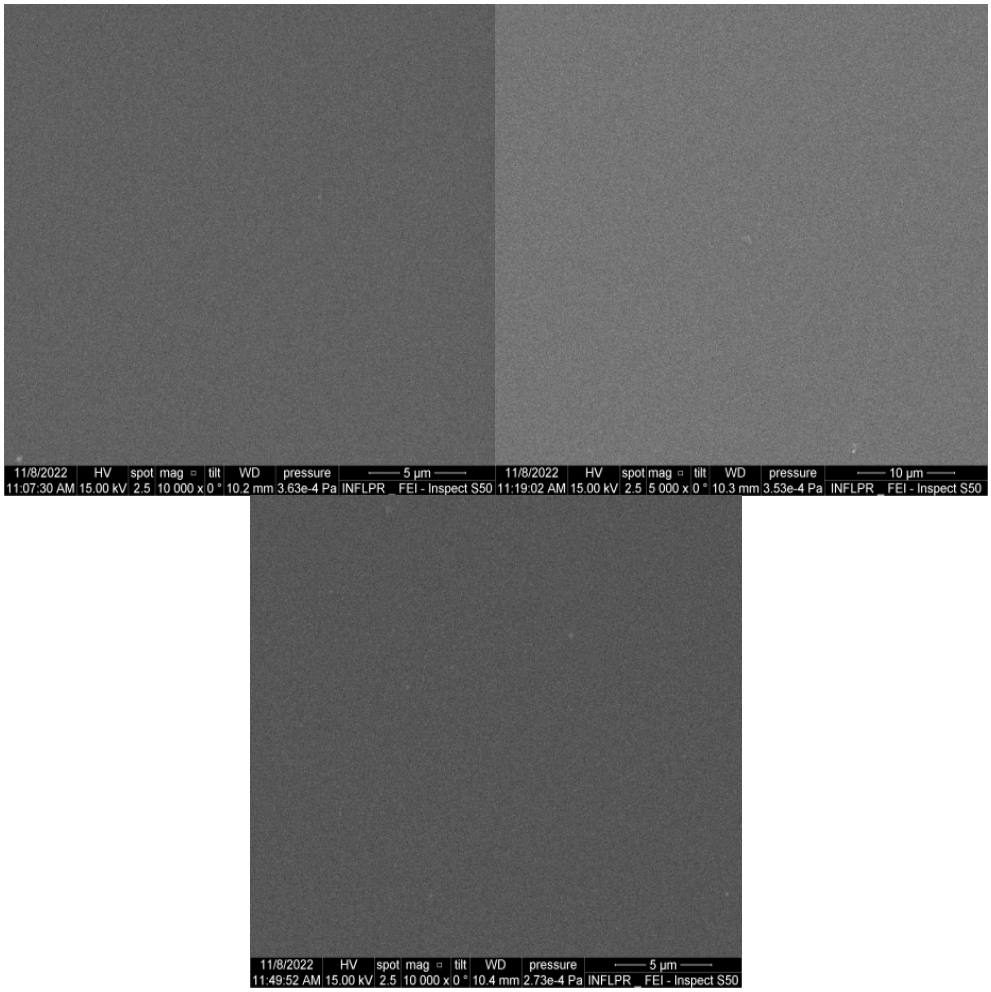

Si_4_A (CrZr),10kx Si_5_A (CrZr), 5kx Si_6_B ($CrZrO_2$), 10kx

Fig. 3. SEM images for samples: Si_4_A (10kx magnification), Si_5_A (5kx magnification), and Si_6_B (10kx magnification).

In some samples, few droplets of around 100nm can be observed, as we can see in Fig.4 for samples Si_1_A (at 5kX magnification), Si_1_B (at 10kx magnification), and Si_4_B (at 1kx magnification). The appearance of particulates is caused by the arching events that occur at target surface during the deposition procces and are more pronounced during reactive sputtering (when O_2 is injected in the reaction chamber).

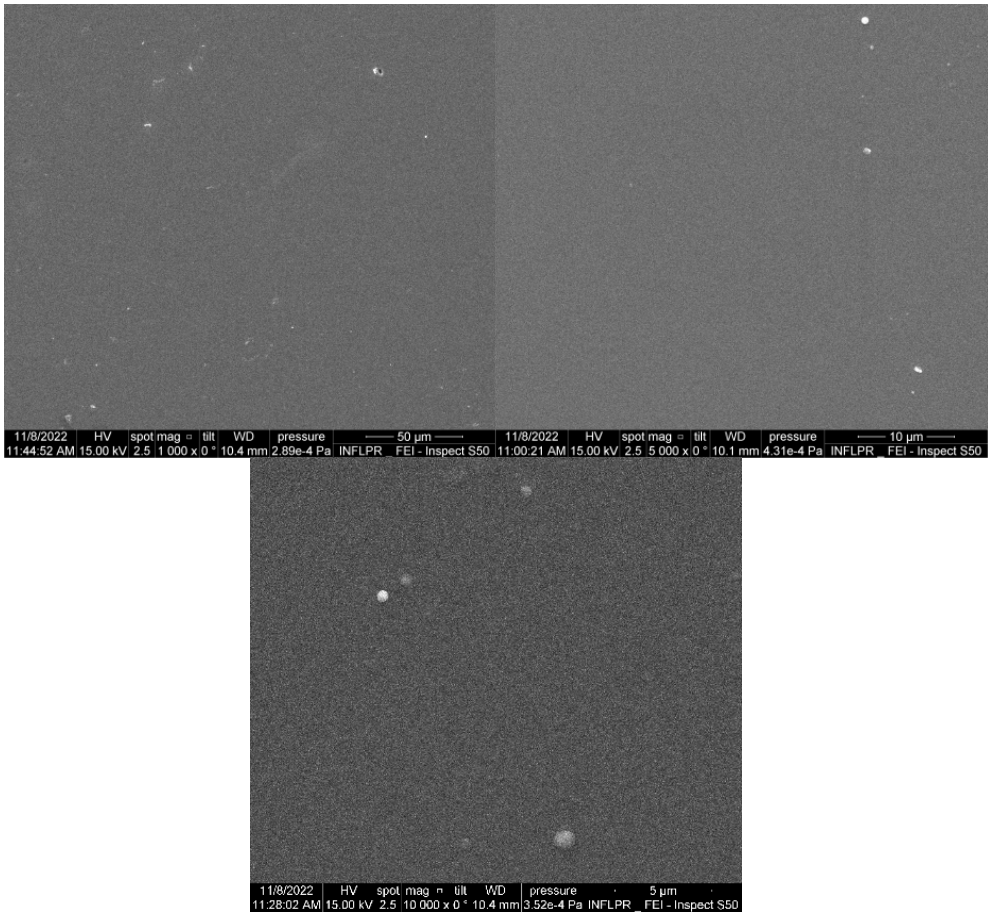

Si_1_A (CrZr), 5kx Si_1_B ($CrZrO_2$),10kx Si_4_B ($CrZrO_2$),1kx

Fig. 4. SEM images for samples: Si_1_A (5kx magnification), Si_1_B (10kx magnification) and Si_4_B (1kx magnification).

The coatings deposited on the carbon substrate present more morphological features as these substrates have a lower grade surface polish finish as to sliced silicon wafers.

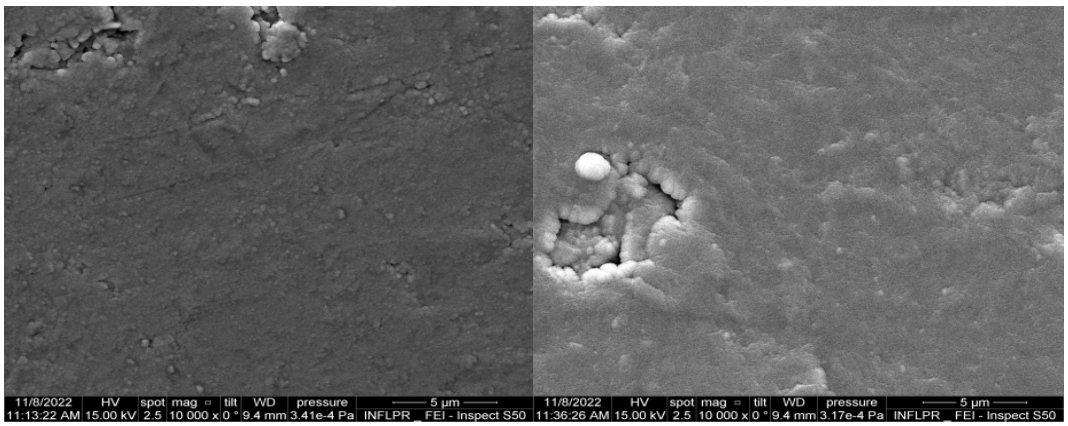

C_3_A (CrZr), 10kX C_3_B ($CrZrO_2$),10kX

Fig. 5. SEM images for samples: C_3_A (10kx magnification) and C_3_B (10kx magnification).

Because of these imperfections, the deposited film tends to follow the substrate topology and cracks can be seen on the surface as shows Fig.5 in the cases of samples C_3_A (at 10kx magnification) and C_3_B (at 10kx magnification).

3.2. Mechanical properties

To investigate the mechanical properties of the samples was used a Bruker nanotender. The Bruker Hysitron TI 980 TriboIndenter uses different types of force and displacement transducers to cause elastic and plastic deformation of samples. Quantitative force measurements allow the system to extrapolate mechanical properties such as Elastic Modulus (Young's Modulus), Hardness, Coefficient of friction and Wear resistance. This makes the system useful for testing samples that require specific testing, such as thin films and nanostructures.

The results obtained from the nanoindentation process will be presented comparatively, thus Si_1_A vs Si_1_B and so on (Tabs.3 and 4), respectively Si_1_A vs. Si_6_A and so on (Tab.3) and Si_1_B vs. Si_6_B and so on (Tab.4), thus comparing both from the point of view of the influence of oxygen and the positioning of the substrate during deposition. In order to have a more accurate picture of the Hardness and Elasticity modulus, several nanoindentations were performed using various types of functions.

Table 3. Comparison of samples obtained from the same batch (A).

Si_1_A		Si_6_A	
Partial Unload	Basic QS Trapezoid	Partial Unload	Basic QS Trapezoid
Young Modulus: 97.77 GPa Hardness:7.55GPa	Young Modulus: 89.7 GPa Hardness: 7.34 GPa	Young Modulus: 41.66 GPa Hardness: 4.79 GPa	Young Modulus: 27.48 GPa Hardness: 5.18 GPa
Si_2_A		Si_5_A	
Partial Unload	Basic QS Trapezoid	Partial Unload	Basic QS Trapezoid
Young Modulus: 10.65 GPa Hardness:1.5 GPa	Young Modulus: 4.47 GPa Hardness: 1.2GPa	Young Modulus:126.27 GPa Hardness: 8.48 GPa	Young Modulus: 118.97 GPa Hardness: 8.66 GPa
Si_4_A			
Partial Unload		Basic QS Trapezoid	
Young Modulus: 103.62 GPa Hardness: 7.73 GPa		Young Modulus: 91.31 GPa Hardness: 7.83 GPa	

Table 4. Comparison of samples obtained from the same batch (B).

Si_1_B		Si_6_B	
Partial Unload	Basic QS Trapezoid	Partial Unload	Basic QS Trapezoid
Young Modulus: 18.32 GPa Hardness: 2.38 GPa	Young Modulus: 9.30 GPa Hardness: 1.93 GPa	Young Modulus: 118.60 GPa Hardness: 11.61 GPa	Young Modulus: 114.40 GPa Hardness: 10.99 GPa
Si_2_B		Si_5_B	
Partial Unload	Basic QS Trapezoid	Partial Unload	Basic QS Trapezoid
Young Modulus: 98.63 GPa Hardness:7.84GPa	Young Modulus: 96.54 GPa Hardness: 7.88 GPa	Young Modulus:108.42GPa Hardness: 8.63GPa	Young Modulus:109.66GPa Hardness: 9.05 GPa
Si_4_B			
Partial Unload		Basic QS Trapezoid	
Young Modulus: 114.29 GPa Hardness: 9.23 GPa		Young Modulus: 111.63 GPa Hardness: 9.00GPa	

The evolution of the Young's Modulus depending on the position during the deposition of A and the evolution of Hardness depending on the position during the deposition of A is presented in Fig.6 and Fig.7 respectively.

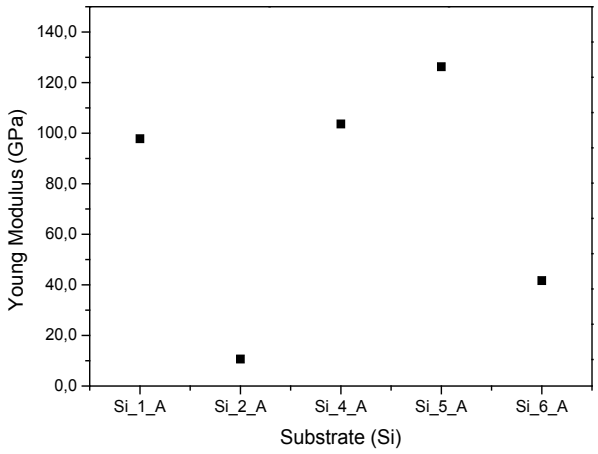

Fig. 6. The evolution of the Young's Modulus depending the position during the deposition of A.

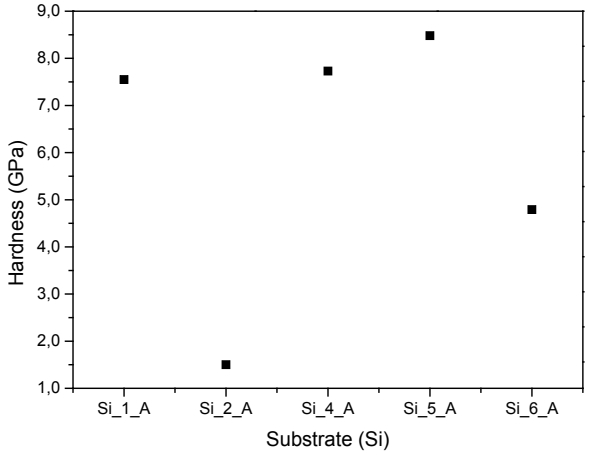

Fig. 7. The evolution of Hardness depending on the position during the deposition of A.

The evolution of the Young's Modulus depending on the position during the deposition of B and the evolution of Hardness depending on the position during the deposition of B is presented in Fig.8 and Fig.9 respectively.

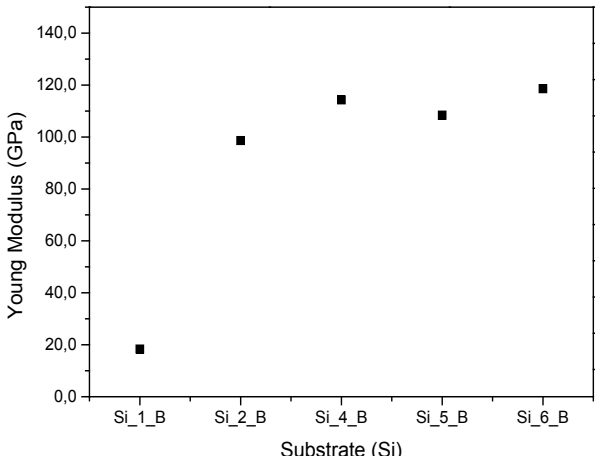

Fig. 8. Evolution of the Young's Modulus depending on the position during the deposition B.

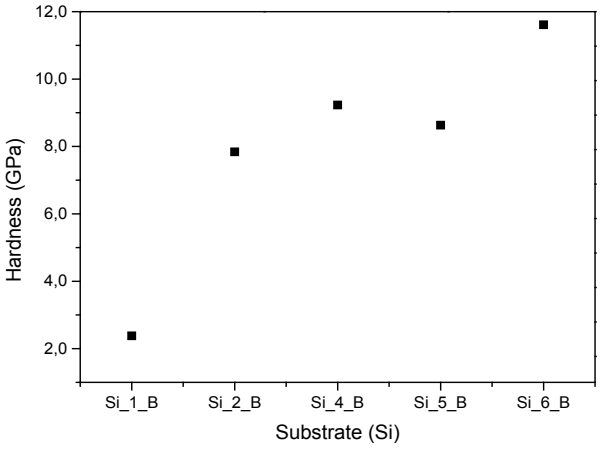

Fig. 9. Evolution of Hardness depending on the position during the deposition B.

Graphic representation of the results obtained for both types of deposition: A (without O_2), B (with O_2) is given for the Yong and Hardness modules in Fig.10 and Fig.11, respectively.

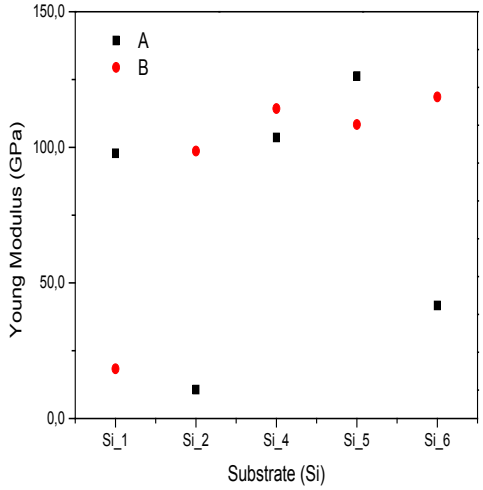

Fig. 10. Evolution of the Young's Modulus depending on the position during deposition.

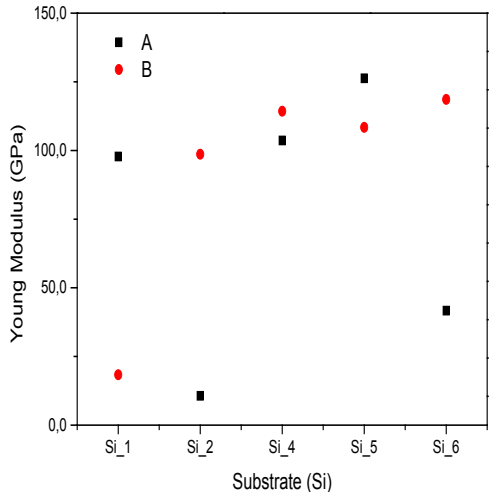

Fig. 11. The evolution of Hardness depending on the position during deposition.

3.2.1. Discutions

The experimental results obtained through nanoindentation studies, in the Partial Unload mode, show: a decrease in both the Elastic Modulus (YM) and the Hardness (H) comparatively (Tab.3, Figs.6 and 7) in the case of samples Si_1_A (YM: 97.77GPa, H: 7.55 GPa) and Si_6_A (YM: 41.66 GPa, H: 4.79GPa), and on the contrary, a comparative increase in the case of samples Si_2_A (YM: 10.65 GPa, H: 1.2GPa) and Si_5_A (YM: 126.27 GPa, 8.48 GPa). Thus, it can be stated that in the absence of oxygen during deposition (Zr-Cr structures), the Modulus of Elasticity and Hardness are influenced by the concentration ratio of the two components Cr and Zr, i.e., there is the practical possibility of adjusting the two parameters YM and H by correspondingly changing the concentrations of the components of the structure.

The presence of Oxygen during the depositions leads to the comparative increase of the YM and H parameters, in the Partial Unload mode, as follows (Tab.8, Figs.5 and 9): an increase in

both the Elastic modulus and the Hardness comparatively in the case of samples Si_1_B (YM: 18.32 GPa, H: 2.38 GPa) and Si_6_B (YM: 118.60 GPa, H: 11.61 GPa), and an comparative increase in the case of samples Si_2_B (YM: 98.63 GPa GPa, H: 7.84 GPa) and Si_5_B (YM: 108.42 GPa, H: 8.63 GPa). It therefore follows that in the case of the Zr-Cr-O structures, the modification of the YM and H parameters as a result of the changes in the concentrations of the components, as expected, are done in a different way than in the case of Zr-Cr, due to the chemical bonds in which Oxygen is involved .

The comparison of results obtained for both types of deposition (Figs. 10 and 11) shows: In the case of the Si_1 sample, the presence of Oxygen causes a decrease of 79.45GPa for YM and respectively a decrease of 5.17GPa for H, under conditions where the concentration of Chromium is maximum and the concentration of Zirconium is minimum, which means that Cr-O bonds are predominant. In all other cases (samples Si_2, Si-4, Si_5, Si_6), the presence of Oxygen causes an increase in the YM and H parameters, the increase being maximum in the case of sample Si_6, in which the concentration of Zirconium is maximum and the concentration of Chromium is minimum, now the bonds Zr-O being predominant (an increase of 76.94GPa for YM and an increase of 6.82GPa for H).

3.3. XRD characterizations

The crystalline structure was investigated using X-Ray Diffraction (XRD) method. The experimental set-up was composed of a diffractometer equipped with a Cu-Kα X-ray sourse, with a specific wavelength of 0.154nm, in a Bragg-Bretano type geometry. The measured range was between 10^0-70^0; an incremental step of 0.02^0 and an integration time per step of 0.7s were used. Figs 12 and 13 show the diffractograms in the case of the Cr-Zr (Si_4_A) sample for short scan 0.2 s integration time per step (0.01^o) and for long scan 0.5 s integration time per step (0.01^o), respectively.

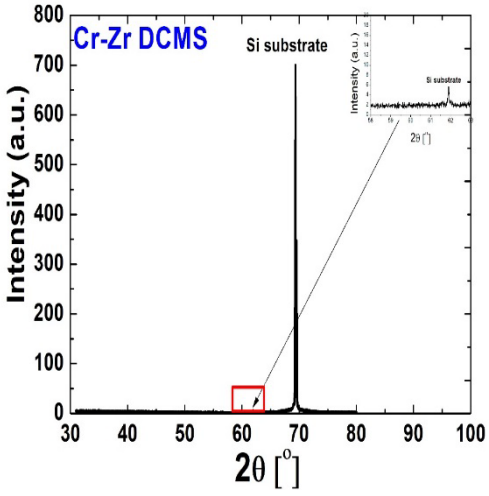

Fig. 12. Diffractogram for Sample Si_4_A (Short scan 0.2 s integration time per step (0.01^o)).

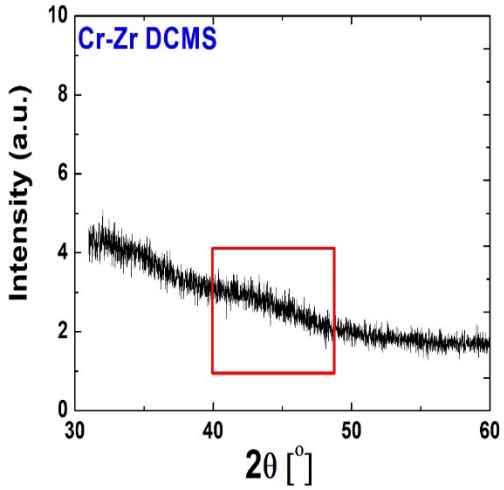

Fig. 13. Diffractogram for Smple Si_4_A (Long scan 0.5 s integration time per step (0.01°)).

From Fig.12 it can be seen that only the peaks corresponding to the Si substrate are visible highlighting the amorphous character of the structure. The amorphous shoulder highlighted in Fig. 13 coincides with the main peaks corresponding to Cr and Zr crystalline phases which can point to amorphous layer growth.

In order to highlight the effect of the element Cr together with Zr and O, the diffractograms of Fig. 14 [6] and Fig. 15 are presented for comparison. Thus, the diffractogram of the ZrO_2 sample (Fig.13[6]) shows three areas.

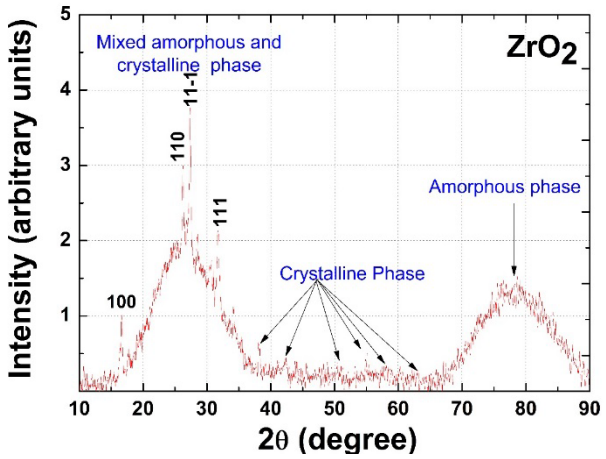

Fig. 14. The diffractogram of the ZrO_2 sample [6].

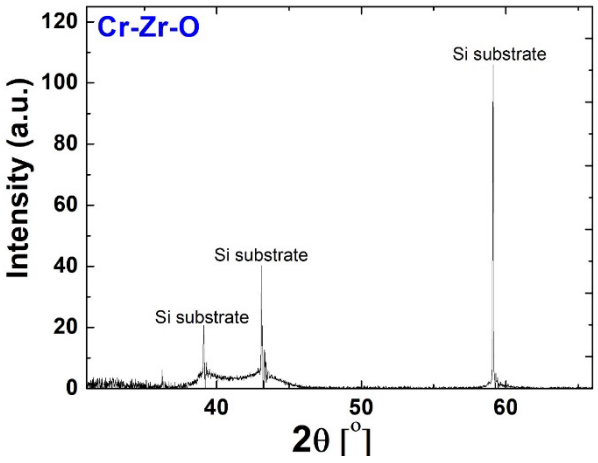

Fig. 15. The diffractogram of the $CrZrO_2$ (Si_4_B) sample.

A first area with a clear degree of amorphization combined with the relative intense orientations of the examinated material, a secund area with many crystalline orientations of low intensity, and a third amorphized area. The identification of the crystalline phases was obtined by comparing the position of the peaks in the diffractogram with the structure files in the Pearson database. The preferential crystallization plane is 11-1. Also, a large number of peaks of low intensity appear in the diffractogram. Considering the application of these materials in dentistry, the 2 wide amorphous strips in the case of ZrO_2 sample (Fig.14) and amorfous character found in the case of Cr-Zr-O sample (Fig.15), could correspond to the adhesive used to attach the veneer to the tooth of such structures. From this perspective, it can be stated that the presence of the Cr element in the Cr-Zr-O structure widens the possibility of its use as an adhesive to attach the veneer to the tooth.

4. Conclusions

The co-depositions of Cr+Zr and those of $Cr+Zr+O_2$ coatings of 500 nm thick were made using magnetron sputtering in continuous mode .The topology of all of the CrZr and $CrZrO_2$ coatings deposited on silicon and carbon substrates have been SEM investigated at three magnifications: 1000x, 5000x and 10.000x. For all of the coatings deposited on Si substrates, at all three magnifications, we observe very smooth surfaces with only small topological elements. In some samples, few droplets of around 100nm can be observed. The appearance of particulates is caused by the arching events that occur at target surface during the deposition proces and are more pronounced during reactive sputtering. The coatings deposited on the carbon substrate present more morphological features as these substrates have a lower grade surface polish finish as to sliced silicon wafers, the deposited film tends to follow the substrate topology and cracks can be seen on the surface.

Were investigated the mechanical properties of the samples obtained after the deposition of Cr+Zr, respectively $Cr+Zr+O_2$. The experimental results obtained through nanoindentation studies, in the Partial Unload mode, show: In the absence of oxygen during deposition (Zr-Cr structures), the Young's Modulus (YM) and Hardness (H) are influenced by the concentration ratio of the two components Cr and Zr, i.e., there is the practical possibility of adjusting the two parameters YM and H by correspondingly changing the concentrations of the components of the structure .

In the case of the $Cr+Zr+O_2$ structures, for sample where the concentration of Chromium is maximum and the concentration of Zirconium is minimum, the presence of Oxygen causes a decrease for YM and respectively a decrease for H (in this case Cr-O bonds are predominant). In the case of sample in which the concentration of Zirconium is maximum and the concentration of

Chromium is minimum, in the presence of Oxygen (now the bonds Zr-O being predominant), an increase for YM and an increase for H are observed.

The crystalline structure was investigated using XRD technology. In the case of the Cr-Zr sample diffractograms show that only the peaks corresponding to the Si substrate are visible, highlighting the amorphous character of the structure. Also, the measurements reveal the amorfous character of the $Cr+Zr+O_2$ sample. In order to highlight the effect of the element Cr together with Zr and O, the diffractogram of the ZrO_2 sample and diffractogram of $Cr+Zr+O_2$ sample are examinated for comparison. Considering the application of these materials in dentistry, the 2 wide amorphous strips in the case of ZrO_2 sample and amorfous character found in the case of $Cr+Zr+O_2$ sample, could correspond to the adhesive used to attach the veneer to the tooth of such structures. From this perspective, it can be stated that the presence of the Cr element in the $Cr+Zr+O_2$ structure widens the possibility of its use as an adhesive to attach the veneer to the tooth.

References

[1] Spitz,S., et al, Surface and Coatings Technology,Volume 237, 25 December 2013, Pages 149-157; https://doi.org/10.1016/j.surfcoat.2013.08.034

[2] M. Åstrand, et al, Surface and Coatings Technology, Volumes 188-189, November-December 2004, Pages 186-192; https://doi.org/10.1016/j.surfcoat.2004.08.021

[3] Landälv, L., et al, Acta Materialia, 131, 543-552(2017); https://doi.org/10.1016/j.actamat.2017.03.063

[4] M. Mohammadtaheri,et al, Surface and Coatings Technology, Volume 375, 15 October 2019, Pages 694-700; https://doi.org/10.1016/j.surfcoat.2019.06.102

[5] Harish C., et al, Applied Surface Science, Volume 255, Issue 5, Part 2, 30 December 2008, Pages 2925-2931; https://doi.org/10.1016/j.apsusc.2008.08.057

[6] V.Ciupina, et al, Journal of Ovonic Research, Vol.18, No.6, November-December 2022, p. 759-767

[7] Liang, R.; Deng, M.; Cui, S.; Chen, H.; Qiu, J. Mater. Res. Bull. 2010, 45, 1855−1860; https://doi.org/10.1016/j.materresbull.2010.09.016

[8] Song, H.; Qiu, X.; Li, F. Appl. Catal., A 2009, 364, 1−7; https://doi.org/10.1016/j.apcata.2009.04.046

[9] Guo, D.; Qiu, X.; Zhu, W.; Chen, L. Appl. Catal., B 2009, 89, 597−601; https://doi.org/10.1016/j.apcatb.2009.01.025

[10] Kai Huang et al, Surface and Coatings Technology,Volume 400, 25 October 2020, 126177; https://doi.org/10.1016/j.surfcoat.2020.126177